Nigerian Research Journal of Engineering and Environmental Sciences 3(1) 2018 pp. 207-216

Nigerian Research Journal of Engineering and Environmental Sciences
Journal homepage: www.rjees.com

Original Research Article

INSULATOR CLASSIFICATION USING SCALE INVARIANT FEATURE TRANSFORM WITH K-NEAREST NEIGHBOUR

***[1]Iruansi, U. and [2]Oyebode, K.O.**

[1]Department of Computer Engineering, Faculty of Engineering, University of Benin, PMB 1154, Benin City, Nigeria.
[2]School of Engineering, University of KwaZulu-Natal, Durban, South Africa.
*uiruansi@gmail.com; kazeemkz@gmail.com

ARTICLE INFORMATION

Article history:
Received 19 May, 2018
Revised 25 May, 2018
Accepted 30 May, 2018
Available online 30 June, 2018

Keywords:
Active contour
Classification
Insulator
K-nearest neighbour
Scale invariant feature transform

ABSTRACT

The demand of uninterrupted supply of electricity is equally increasing the need to monitor the electric power grid. Insulators are part of the components that make up the electric power grid. Hence, faulty insulators may affect the mechanical and electrical performance of an electric power grid, which can lead to the flow of leakage currents through the line supports. The traditional method of inspection is inadequate in meeting the growth and development of the present electric power grid. Hence an automated system such as the computer vision method is presently being explored as a means to resolve this crisis safely, speedily and accurately. This paper presents a method of insulator classification using scale invariant feature transform and k-nearest neighbor. The case study validates the efficacy of the proposed methodology for insulator classification.

1. INTRODUCTION

Insulators are vital components in the power grid because they are materials used to hold electrical conductors and also to prevent electric current from flowing through them. There are different kinds of insulator materials namely polymer, glass and porcelain. This study is based on polymeric insulators which is commonly used in outdoor installations by the traditionally cautious electric power utilities worldwide (Gencoglu, 2007). The tremendous growth in the application of the polymeric insulator is as a result of its characteristics. These include light weight, less load to the supporting structure due to its light weight, high-tensile strength, high performance in polluted areas and better withstand voltage than porcelain or glass insulators (Gencoglu, 2007). In the power grid, faulty insulators cause major effect on the transmission and distribution of electricity. Such effects include voltage drop, leakage currents flow, and losses to the power grid (Xinye et al., 2010; Iruansi et al., 2015). Hence, there is a need for early detection of faulty insulators in order to reduce outages and maintain or increase the performance of the power sector.

Inspection in the power grid is usually carried out manually, either from the lines or from the ground or air using vehicle or helicopter respectively. This manual method endangers the life of the inspector since the environment of the insulators are dangerous with high potential difference between the lines generating an electric and magnetic field in the region of lines at normal condition and higher in the presence of defects (Katrasnik et al., 2008). With the traditional method of inspection, on-site insulator condition is not only expensive, tedious and time consuming, but almost impossible to monitor and inspect long lines spanning through long distance with difficult terrain. Thus, a better approach to power grid inspection is the use of a robot which can move along the lines with its design to overcome barriers on the lines. The main advantage of the robot is its proximity to object of interest and its low vibration, which increases the inspection accuracy and the quality of image acquisition respectively. Therefore, image processing and computer vision method have been recognized as a means to determine the condition of insulator safely, speedily and accurately. Image processing and computer vision methods are less expensive because of the current technological development in the field of digital imaging and the availability of inexpensive cameras. Therefore, images captured with digital cameras along the power-lines can be sent to the control room for further analysis. Insulators are just part of the whole power-line delivery system. It means that in order to assess the condition of an insulator, it must first be extracted from the context. This will involve image segmentation in order to identify the region of interest. Thereafter, features characterizing the condition of the insulator are considered and are extracted and then fed into a classifier to determine the condition of the insulator.

Presently, there are few researches on insulator condition or status using image processing and computer vision. For insulator fault detection, Ge et al. (2006) and Mei et al. (2012) proposed insulator dirt detection for high resolution images. Both methods employed colour model for dirt detection. Colour model is not a robust method for cracks and broken parts. Also, images were captured at a very close range showing just a single cap of an insulator unlike our images showing the complete insulator. A simple method was proposed by (Xinye et al., 2010), that uses colour thresholding for insulator recognition. This method is not robust because it needs a well-adjusted threshold parameter which can be a limitation. Other researchers used different feature extraction methods and classifiers with promising results (Murthy et al., 2010; Murthy et al., 2011; Reddy et al., 2011; Reddy et al., 2013). Also, Prasad and Rao (2016) used local binary pattern in combination with histogram Fourier (LBP-HF). In this paper, the research is based on the use of Scale Invariant Feature Transform (SIFT) with K-Nearest Neighbour (KNN). From the preceding, it is intuitive that an automated algorithm which is fast, safe and accurate is vital for insulator condition. Hence, this work presents an automated algorithm for classification of defectuous and non-defectuous power-line insulators.

2. MATERIALS AND METHODS

2.1 Pre-processing

In order to reduce noise and improve the quality of images, pre-processing step was used. Colour images in Red, Green and Blue (RGB) representation were converted into grey scale images. Then, morphological operation using top-hat filter was applied to enhance images (Jalba et al., 2004). The top-hat filter is defined as:

$$T(I) = I - (IoS) \tag{1}$$

where I is the insulator image in grey-scale, S is the structuring element which is an open disk and o denotes the opening operation which is the dilation of the erosion of a set M by a structuring element S, the opening operation is defined as $[MoS = (M\Theta S) \oplus S]$. The symbols Θ and $\oplus$ denotes erosion and dilation respectively. The top-hat images obtained were further enhanced by the application of morphological operation known as dilation (Gonzalez et al., 2004). Dilation is defined as:

$$(I_d \oplus S)(u,v) = \max[I_d(u-u^i, v-v^l) - S(u^i, v^l)(u^i, v^l) \in D_S \quad (2)$$

Where I_d is the image and *Ds* is the domain of the structuring element *S*, and (*u,v*) are pixel coordinates.

The output image of the dilated image was subtracted from the original grey level insulator image for further analysis on insulator segmentation. The subtracted image is defined as:

$$I_S = I - I_d \quad (3)$$

2.2. Insulator Segmentation

After insulator pre-processing, insulator segmentation was done using Active Contour Model (ACM) in order to extract insulator region of interest (ROI) (Chan and Vese, 2001). ACM has been extensively used in image segmentation such as (Chan and Vese, 2001; Iruansi et al., 2015). ACM is based on energy function expressed in-terms of level set function φ defined as:

$$\begin{aligned} E(k_1, k_2, \varphi) = {} & \lambda_1 \int_\Omega (1-k_1)^2 H(\varphi) dx \\ & + \lambda_2 \int_\Omega (1-k_1)^2 (1-H(\varphi)) dx \\ & + \mu \int_\Omega |\nabla H(\varphi)| \, dx \end{aligned} \quad (4)$$

where φ is the level set function, Ω is an open bounded region with foreground Ω_1, background Ω_2. λ_1, λ_2 and μ are fixed parameters. Then, Heaviside step function H, and mean intensities k_1 and k_2 are defined as:

$$k_1(\varphi) = \frac{\int_\Omega (I(u) H(\varphi(u)) du}{\int_\Omega H(\varphi(u)) du} \quad (5)$$

$$k_2(\varphi) = \frac{\int_\Omega (I(u)(1-H(\varphi(u))) du}{\int_\Omega (1-H(\varphi(u))) du} \quad (6)$$

$$H(\varphi) = \begin{cases} 1 & if \quad \varphi \geq 0 \\ 0 & if \quad \varphi < 0 \end{cases} \quad (7)$$

where φ is zero if it is at the boundary of the curve or greater than zero if it is inside the curve or less than zero if it is outside the curve.

From Equation (4), the first term is a measure of the variance of the background grey level in regards to pixel intensity in the image, the second term is a measure of the variance of the insulator (foreground) grey level based on the measure of uniformity of pixel intensity in the image and the third term expresses the length of the boundary of the insulator in the image *I*. The Heaviside function determines the insulator image and the background regions in the observed image *I*. Thus, to segment insulator from an image, Equation (4) was minimized with respect to k_1, k_2 and φ. With φ constant, the mean grey values of k_1 and k_2 were computed with Equations (5) and (6) respectively. Also, with k_1 and k_2 constant using calculus of variations for Equation (4), the gradient decent equation for the evolution of φ is derived as:

$$\frac{\partial \varphi}{\partial x} = \delta(\varphi)\left[\mu\nabla \bullet (\nabla\varphi/|\nabla\varphi|) - \lambda_1(1-k_1)^2 + \lambda_2(1-k_2)^2\right] \quad (8)$$

where $\nabla.(\nabla\varphi/|\nabla\varphi|)$ is the curvature of the curve, that provides smoothing constraints during curve evolution thereby minimizing the total curvature of the contour. The Dirac measure is applied in order to work very close to the minimization problem. The Dirac measure is defined as:

$$\delta(\varphi) = \frac{d}{d\varphi}H(\varphi) \quad (9)$$

2.3. Region of Interest

Insulator region of interest was extracted by first extracting the coordinates and size of the insulator (foreground pixels) from the segmented image. Then, the extracted coordinates and size of the segmented image were mapped into the original grey scale image of same size with the segmented image. The mapped coordinates were used to determine the minimum bounding box over the entire insulator for the extraction of insulator ROI

2.4. Algorithm of Insulator Segmentation and Region of Interest

Algorithm 1 gives the steps for insulator segmentation and extraction of insulator region of interest.

Algorithm 1: Insulator Segmentation and ROI

Require: *I*. Source Image
Ensure: *E*. Extracted Image of Insulator ROI

1: Convert the original colour image *I* into grey scale and save result as *g*
2: Define a structuring element *s*
3: Apply Equation (1) on g and save result as *T*
4: Apply Equation (2) on *T* and save result as T_d
5: Apply Equation (3) and save result as I_s
6: Initialize a level set function φ
7: for $n = 1$ to maximum value of *n* do
8: Compute $k_1(\varphi)$ and $k_2(\varphi)$ using Equations (5) and (6) respectively
9: Compute φ^{n+1} by the discretization and linearization of Equation (8)
10: Check whether curve is stationary
11: if curve is stationary then
12: Escape from the for loop
13: end if
14: end for
15: Save segmented image as *sIm*
16: Extract coordinates of the ROI from *sIm*
17: Map the coordinates from *sIm* on *g*
18: Extract insulator ROI from *g* and save as *E*
19: End

2.5. Feature Extraction using SIFT

SIFT algorithm (Lowe D.G. 2004) is used for feature extraction. The features are less sensitive to scale, translation and rotation. The stages of the SIFT algorithm are scale space extrema detection, keypoint localization, orientation assignment and keypoint descriptor generation.

Scale space extrema: The scale space is the first stage of SIFT algorithm which searches all scales over several octaves of image. It is implemented by using Difference of Gaussian (DoG) to identify potential keypoints that are invariant to scale and image rotation. In the scale space extrema detection phase, the SIFT algorithm computes the "scale", DoG, and extrema over several "octaves". The computation of scale space is defined as:

$$S_p(u,v,\sigma) = G_\alpha(u,v,\sigma) * I(u,v) \tag{10}$$

Where $I(u,v)$ is the image, $*$ denotes convolution operator for two-dimensional at point (u,v) and $G_\alpha(u,v,\sigma)$ represents the Gaussian function for image blurring.

The SIFT algorithm was repeatedly used to compute the scale of the image, which then produced a sequence of scales known as octave. In the next step, all these octaves were used to generate the DoG images. The DoG can be computed by subtracting each adjacent image with a multiplication factor of *m* and it is derived as:

$$D(u,v,\sigma) = S_p(u,v,m\sigma) - S_p(u,v,m\sigma) \tag{11}$$

Keypoint localization: After the comparison of pixel with its neighbouring pixel to obtain keypoint candidate (extrema), the next step was an interpolation of nearby data for location, scale, and ratio of principal curvatures. This information allows points to be rejected which have low contrast or that are poorly localized along an edge. The interpolation was performed using the quadratic Taylor expansion of the DoG scale-space function, $D(u,v,\sigma)$ with the keypoint candidate as the origin. In order to increase stability, since rejection of keypoints with low contrast was not a sufficient means, keypoints were eliminated with poorly determined locations but with high edge responses. Thus, to detect the extrema on edges, the principal curvature was used and computed from a *2x2* Hessian matrix, *H*, at the location and scale of the keypoint. The *2x2* Hessian matrix is defined as:

$$H = \begin{bmatrix} D_{uu} & D_{uv} \\ D_{uv} & D_{vv} \end{bmatrix} \tag{12}$$

Then, the trace and determinant of *H* were computed for the generation of the ratio for principal curvature. This quantity was compared with a threshold value to determine if an extremum is to be discarded or not. After the elimination of extrema points, the remaining points were the keypoints.

Orientation assignment: At this stage, the main aim is to achieve invariance to image rotation. The magnitude $m(u,v)$ and rotation $\theta(u,v)$ for each pixel in a neighbouring region around the keypoint in the Gaussian smoothed image *S(x; y)* at this scale, can be computed as:

$$m(u,v) = \sqrt{(S_p(u+1,v) - S_p(u-1,v))^2 + (S_p(u,v+1) - S_p(u,v-1))^2} \tag{13}$$

$$\theta(u,v) = \tan^{-1}((S_p(u,v+1) - S_p(u,v-1))/(S_p(u+1,v) - S_p(u-1,v))) \tag{14}$$

Then an orientation histogram was generated that has 36 bins covering a 360 degree range of orientations. The peaks in the histogram correspond to the pre-eminent orientations of local gradient and the orientation detected as the highest peak in the histogram. For any other local peak that is within 80% of the highest peak, a keypoint was created with that orientation.

Keypoint descriptor generation: In this stage, a descriptor vector was computed for each keypoint such that the descriptor is highly distinctive and partially invariant to illumination and 3D viewpoint. The descriptor vector was computed as a set of orientation histograms on *4x4* pixel neighbourhoods with 8-bins. These histograms were computed from the magnitude and orientation values of a *16x16* region around the keypoint, with each histogram having a *4x4* sub-region of the original region. The magnitudes were further weighted using a Gaussian function and the width of the descriptor window was based on the value of sigma in the Gaussian function. With a *4x4 = 16* histogram, each histogram has 8-bins and a vector of 128 elements. Thus, for invariance to affine changes in illumination, the vector was normalized to a unit length.

2.6. Classification using K-Nearest Neighbour

K-nearest neighbor was first proposed by Fix and Hodges as a non-parametric method of classification which is based on the "distance" between points or distribution. In KNN classification, an object is classified into a class with majority vote within the KNN. The extracted feature vectors were fed into a KNN classifier in order to classify insulators as defectuous and non-defectuous. Typically, KNN is used to train a set of feature vectors or attribute vectors with a given corresponding class label in order to predict a class of an unknown instance *x*. An instance *x* relates to a point in an n-dimensional space and can be represented by an attribute vector $\left[v_1(x), v_2(x),..., v_n(x)\right]$, where *n* is the number of attributes. In our case, KNN used the Euclidean distance to measure the distance between instance x_i and x_j. The Euclidean distance is defined as:

$$d(x_i, x_j) = \sqrt{\sum_{m=1}^{n} (v_m(x_i) - v_m(x_j))^2} \tag{15}$$

Given a new instance *y*, KNN uses the k-nearest instance in the training set i.e. $x_1, x_2,..., x_k$, thereby returning the result of classifying *y* as defined as:

$$c(y) \leftarrow \arg \max_{c \varepsilon C} \sum_{r=1}^{k} \delta(c, c(x_i)) \tag{16}$$

where *c(y)* is the class of the instance *y, k* is the number of neighbours, *C* and *c* represents the class variable and $\delta(c, c(x_i))$ is equal to 1, if *c* is equal to $c(x_i)$ and 0 otherwise.

2.7. Algorithm for Insulator Classification

Algorithm 2 gives the steps involved in insulator classification using SIFT with KNN.

Algorithm 2: Insulator classification using SIFT with KNN

Require: Dataset. Training and test set
Ensure: Output. Indicates insulator condition
1: for each image *I* in the training set do

2: Convert each RGB image I into grey scale and save result as g
3: Generate a scale space from g using equation (10)
4: Find key-points or interest points using equation (11)
5: Reject low contrast and bad key-points using equation (12)
6: Assign orientation to the key-points using equations (13) and (14)
7: Generate SIFT key-point descriptor as *D*
8: end for
9: Feed extracted features *D* into KNN classifier for training
10: for image *T* from the test set images do
11: Apply algorithm 1 to each image *T* and save result as *g*
12: Partition image g into four parts and save them into I_p,
13: for $n = 1$ *to* $n = 4$ do
14: Generate a scale space from each image saved into I_p using equation (10)
15: Find key-points or interest points using equation (11)
16: Reject low contrast and bad key-points using equation (12)
17: Assign orientation to the key-points using equations (13) and (14)
18: Generate SIFT key-point descriptor as *D*
19: Save each *D* from I_p result as $S_p(n)$
20: Use the $S_p(n)$ to generate the feature vector *N(n)*
21: Compare extracted features of partitioned images *N(n)* to the trained set *M* if it matches
22: if any label of *N(n),* has a label that is defectuous then
23: Output image T is defectuous
24: else
25: Output image T is non-defectuous
26: end if
27: end for
28: end for

3. RESULTS AND DISCUSSION

The experiment was conducted on a polymeric insulator. The dataset contained 600 insulator images of both defectuous and non-defectuous insulators. The training set was made up of 200 defectuous and 200 non-defectuous insulator images (Figure 1). For the training set, a 10-fold cross validation was applied. The test set is made of 200 insulator images with 100 defectuous and 100 non-defectuous insulator images.

Due to a high signal to noise ratio such as shadows and illumination in the captured images, all insulator images were pre-processed before further analysis. Figure 2(a) shows the original grey-scale images; Figures 2(b) - (d) show the results of the preprocessed stages.

Figure 2(e) shows the result of the application of ACM, where a line is drawn on the boundary of the insulators and the segmented image as shown in Figure 2(f). In cases with some background pixels inside the insulator (foreground), post-processing was employed to fill up the holes.

Figure 2(g) shows the identification of insulator ROI. Figure 2(f) shows the bounding box over the insulator, followed by the extraction of the insulator ROI from the image in Figure 2(a). The output is shown in Figure 2(h). Due to the length of each insulator, it will be difficult to detect some smaller regions that are defectuous, therefore each insulator image is partitioned into smaller segments to enhance classification performance. Figure 2(i) shows an insulator image that has been partitioned.

Tables 1 and 2 show the condition of insulators based on cross validation (CV) and test set implementation outputs respectively. The accuracy of the proposed model is computed using the statistical criteria in (Powers, 2011). The accuracy is defined as:

$$Acc(\%) = (TP + TN)/(TP + TN + FP + FN) \quad (17)$$

where TP is true positive, TN is the true negative, FP is the false positive and FN is false negative.

In the classification phase, a cross validation process was performed in order to predict or optimize the model parameter (such as the regularization parameter and kernel width) to fit the training set. A k-fold cross-validation randomly partitions the training set into k-equal sized subset, whereby a single subset is retained as a test set and all other subsets are used as the training set. Then the cross-validation process is repeated based on the number of fold (k) times, with the k subset used once as the validation set. Thereafter averaging the k results of all folds to obtain a single result. However, the number of fold is 10 and the accuracy is computed using Equation (17). The accuracy obtained for the training set with 10-fold cross validation is *100%* and for the test set is *87%*.

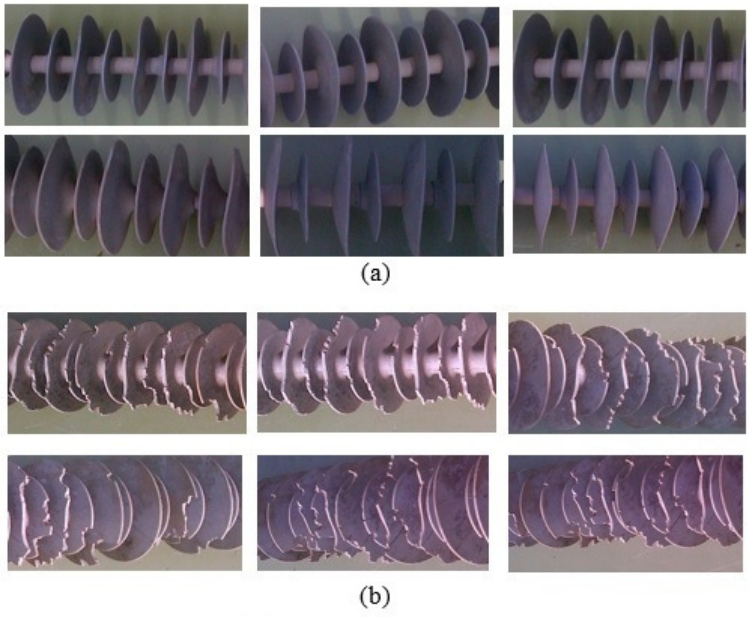

Figure 1: Sample of dataset of non-defectuous and defectuous insulators

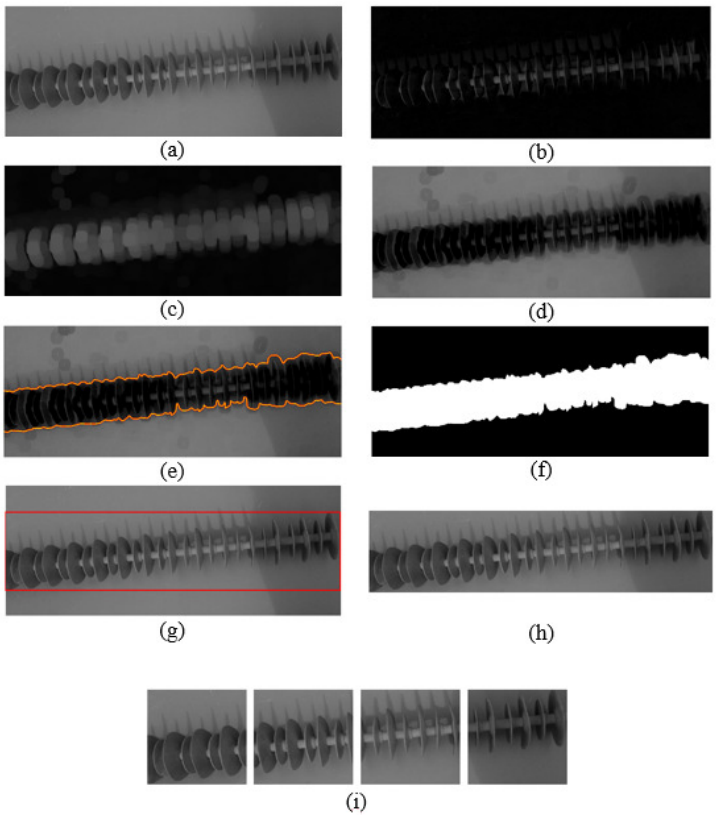

Figure 2: (a) Greyscale image, (b) Top-hat Filtering (c) Morphological dilation (d) Image subtraction (e) ACM (f) Segmented image (g) ROI (h) ROI extraction (i) Partitioned image. Best viewed in colour

Table 1: Confusion matrix for the cross validation

	Defectuous	Non-defectuous
Defectuous	200	0
Non-defectuous	0	200

Table 2: Confusion matrix of the test set

	Defectuous	Non-defectuous
Defectuous	95	5
Non-defectuous	21	79

4. CONCLUSION

In this paper, classification of power-line insulator condition has been investigated and presented. From the results, it is evident that the SIFT is statistically robust, more stable and less prone to noise. In the future, other methods of feature extraction should be implemented and compared with our proposed method that has been established as a baseline. Also, consideration of the integration of insulator condition in real-time system should be established.

5. CONFLICT OF INTEREST

There is no conflict of interest associated with this work.

REFERENCES

Chan, T.F. and Vese, L.A. (2001). Active contours without edges. *IEEE Transactions on image processing*, 10(2), pp. 266–277.

Ge, Y., Li, B., Zhao, S. and Pang, C. (2006). Detection of the insulator dirtiness based on the computer vision. *In China International Conference on Electricity Distribution (CICED 2006)*. IET, pp. 173–176.

Gençoglu, M.T. (2007). The comparison of ceramic and non-ceramic insulators. *Engineering Sciences*, *2*(4), pp. 274-294.

Gonzalez, R.C., Woods, R.E. and Eddins, S.L. (2004). Digital image processing using MATLAB. *Pearson Education India.*

Iruansi, U., Tapamo, J.R., and Davidson, I.E. (2015). An active contour approach to insulator segmentation. *In Proceeding of the 12th IEEE-AFRICON International Conference. IEEE*, pp. 1–5.

Jalba, A.C., Wilkinson, M.H. and Roerdink, J.B. (2004). Morphological hat transform scale spaces and their use in pattern classification. *Pattern Recognition*, 37(5), pp. 901–915.

Katrasnik, J., Pernus, F. and Likar, B. (2008). A climbing-flying robot for power line inspection. *In: Proceedings of the IEEE Conference on Robotics, Automation and Mechatronics. IEEE*, pp. 95–110.

Lowe, D.G. (2004). Distinctive image features from scale-invariant keypoints. *International Journal of Computer Vision,* 60(2), pp. 91-110.

Mei, X., Lu, T., Wu, X. and Zhang, B. (2012). Insulator surface dirt image detection technology based on improved watershed algorithm. *In: Asia Pacific Power and Energy Engineering Conference (APPEEC)*. IEEE, pp. 1–5.

Murthy, V.S., Gupta, S. and Mohanta, D.K. (2011). Digital image processing approach using combined wavelet hidden markov model for well-being analysis of insulators. *IET Image Processing,* 5(2), pp. 171–183.

Murthy, V.S., Tarakanath, K., Mohanta, D.K. and Gupta, S. (2010). Insulator condition analysis for overhead distribution lines using combined wavelet support vector machine (SVM). *IEEE Transactions on Dielectrics and Electrical Insulation,* 17(1), pp. 89–99.

Powers, D.M.W. (2011). Evaluation: from precision, recall and f-measure to roc, informedness, markedness and correlation. *Journal of Machine Learning,* 2(1), pp. 37–63.

Prasad, P.S. and Rao, B.P. (2016). LBP-HF features and machine learning applied for automated monitoring of insulators for overhead power distribution lines. *In: International Conference on Wireless Communications, Signal Processing and Networking (WiSPNET). IEEE*, pp. 808–812.

Reddy, M.J.B., Chandra, B.K. and Mohanta, D.K. (2011). A DOST based approach for the condition monitoring of 11 kv distribution lineinsulators. *IEEE Transactions on Dielectrics and Electrical Insulation,* 18(2), pp. 588–595.

Reddy, M.J.B., Mohanta, D.K, and Chandra, B.K, (2013). Condition monitoring of 11kV distribution system insulators incorporating complex imagery using combined DOST-SVM approach. *IEEE Transactions on Dielectrics and Electrical Insulation,* 20(2), pp. 664–674.

Xinye, Z., An, J. and Chen, F. (2010). A method of insulator fault detection from airborne images, *in Second WRI Global Congress on Intelligent Systems,* 2(1). IEEE, pp. 200–203.